Surface Science 602 (2008) 2278–2283

Contents lists available at ScienceDirect

Surface Science

journal homepage: www.elsevier.com/locate/susc

Particle aggregation on dewetting solid water films

J.S. Palmer, S. Sivaramakrishnan, P.S. Waggoner [1], J.H. Weaver *

Department of Materials Science and Engineering, University of Illinois at Urbana-Champaign, 1304 West Green Street, Urbana, IL 61801, USA

ARTICLE INFO

Article history:
Received 27 February 2008
Accepted for publication 7 May 2008
Available online 13 May 2008

Keywords:
Islanding
Amorphous solid water
Buffer-layer-assisted growth
Thin-ice films

ABSTRACT

Solid water films are used to create a wide range of nanostructures through buffer-layer-assisted growth. Metal atoms vapor-deposited onto solid water films form clusters that aggregate as the film is heated. The aggregation process is driven by the dewetting, islanding, and sublimation of the ice films. The sizes, shapes, and densities of the resulting nanostructures are determined by the formation of ice islands whose sizes and densities are controlled by the thickness of the ice film.

1. Introduction

The importance of water and its elusive properties have assured that the study of condensed water remains a very active area of investigation [1]. Not surprisingly, the interaction of water with metal surfaces has been extensively investigated [2,3]. Much less is known about the inverse systems, in which metal atoms are deposited and form particles on solid water.

Recent studies have shown that nanoparticles are formed when noble metals are vapor deposited onto solid water films condensed on oxide substrates [4–6]. This use of water as a buffer extends a technique introduced by Waddill et al. [7] that is now known as buffer-layer-assisted growth or BLAG [8]. In BLAG, a gas, typically Xe, is condensed onto a cold substrate to form a buffer layer. Material deposited onto the buffer results in three-dimensional clustering as a result of the weak interaction between the buffer and the deposited material. Heating allows sublimation of the buffer and delivery of the clusters to the substrate in the ultimate of soft-landing. BLAG makes it possible to prepare a wide range of nanostructure/support systems that cannot be formed by conventional deposition. Moreover, the sizes and densities of the nanostructures produced with BLAG can be varied over more than two orders of magnitude by changing the buffer thickness and the amount of material [8,9].

In contrast to rare gas films, the structure of solid water films used for BLAG depends strongly on their deposition kinetics. Water condensed at temperatures below 110 K forms amorphous solid water (ASW), a nonequilibrium state stabilized by kinetics; condensation above ~130 K produces crystalline cubic ice (I_c) [10]. Moreover, the porosity of ASW films condensed by exposure to water vapor increases significantly with decreasing condensation temperature below 90 K [11]. ASW films heated through ~135 K undergo a glass transition. The nature of water above this transition is still an issue of active debate, but isotope intermixing [12] as well as microscopy measurements [13] indicate that significant diffusion is occurring. Increasing the temperature above ~150 K results in the conversion to I_c through nucleation and growth of crystallites. This restructuring could play a critical role in the aggregation of particles during BLAG with H_2O, and we have undertaken an investigation of the properties of these films.

In this paper, we demonstrate that particle assembly and aggregation on a solid water buffer layer is controlled by dewetting, islanding, and sublimation of the solid water film. Compared to noble gas buffers, there are differences both in the dewetting of the film and the interactions of the particles with the dewetting front. The interactions of particles with H_2O alter their aggregation and coalescence, and this is reflected in structures produced for Au, Cu, and Pd deposition onto ASW.

2. Experiment

The samples were grown in a chamber with a typical base pressure below 1×10^{-10} Torr. The substrates were 20–30-nm-thick amorphous carbon (a-C) foils supported on copper grids that were degassed *in vacuo* for ~24 h at 125–150 °C. The samples were fixed to copper holders that were mounted on the cold head of a closed-cycle He refrigerator to cool the samples to 20 K; the temperature was measured with a silicon diode (Lakeshore SD-470-SD) attached to the copper holder. The actual temperature at the sample

* Corresponding author. Tel.: +1 217 333 1440; fax: +1 217 333 2737.
E-mail address: jhweaver@uiuc.edu (J.H. Weaver).
[1] Present address: School of Applied and Engineering Physics, Cornell University, Ithaca, NY 14853, USA.

0039-6028/$ - see front matter © 2008 Elsevier B.V. All rights reserved.
doi:10.1016/j.susc.2008.05.003

is estimated to be within 5 K of that reported. Condensation at higher temperatures was achieved by turning off the refrigeration and allowing the cold head to slowly warm up. This results in a heating rate of 1 K/minute at 135 K. After condensation, the refrigeration system was again engaged to cool the sample to 20 K. The buffer was desorbed by removing the sample holder from the coldhead with a stainless steel manipulator, which could be precooled by contact with the coldhead. Upon removal, the temperature rose to 50 K in 10 s and to 100 K in 70 s. Desorption occurred in the range of 150–170 K during which time the heating rate was 1.9 K/min.

Water was condensed by back filling the chamber to 1×10^{-6} Torr using a precision leak valve. The water was purified through multiple freeze and pump cycles using liquid nitrogen. The thicknesses of films grown at 20 K were determined by the exposure time and flux. The number of absorbed molecules per unit time per unit area is $I = s \cdot p/(2\pi mkT)^{1/2}$, where p is the H_2O partial pressure, m is the mass of a water molecule, T is the ambient temperature, k is the Boltzmann constant, and s is the sticking coefficient. The layer thicknesses are given in monolayers (ML), where 1 ML refers to the number of molecules in a (1 1 1) plane of I_c, 1.15×10^{15} cm^{-2}. At 20 K, we assume s to be 1 so that 1 ML corresponds to 2.45 L [14]. For films condensed at higher temperature, thicknesses were estimated by comparison of the pressure during desorption of the film with that of films condensed at lower temperatures. The pressure during desorption was monitored with an ion gauge; the maximum pressure for a 120 ML film was about 8×10^{-8} Torr. The area under the desorption peak of the pressure–time curve increased linearly with film thickness and provided a reliable measure of film thickness. Although desorption occurred from the sample holder and sample, differences in film thicknesses resulting from the first layer sticking coefficient are assumed to be negligible for thick films. The area under the desorption peak was also used to estimate the fraction of the buffer desorbed at different temperatures.

Metal atoms were evaporated onto the buffer layers from a tungsten basket located ~32 cm from the samples. The thickness was determined using a calibrated quartz crystal oscillator. Samples removed from the coldhead were displaced ~2 cm, keeping the distance from the evaporation source constant. The impinging atoms were sufficiently mobile that they could form clusters, a process favored by weak bonding with the solid buffer. The clusters aggregated when the sample was removed from the cold head to desorb the buffer.

Characterization of the samples was done at room temperature after their transfer to a Philips CM12 120-kV or JEOL 2010 LaB_6 200-kV transmission electron microscope (TEM). Imaging was done in the bright-field mode, keeping the beam intensity low to avoid significant changes in morphology. The samples were stable when stored in air, and there was no evidence of coarsening.

3. Metal particles formed on solid water buffers

Contrary to expectations, the deposition of metals onto different thicknesses of H_2O and the subsequent buffer sublimation produces structures very similar to those formed using Xe buffers. Fig. 1 shows representative images for depositions of 5 Å of Au, 5 Å of Cu, and 3 Å of Pd on 10 and 30 ML ASW films. The 10 ML buffers result in small, high-density particles. The 30 ML buffers result in more aggregation and the formation of larger, ramified structures. As structures become larger, the time required for coalescence increases and the driving force decreases [15] such that the aggregates remain ramified even at 300 K. The shapes of the particles vary significantly, depending upon the coalescence properties of the metal. The Au particles in Fig. 1a are compact and have

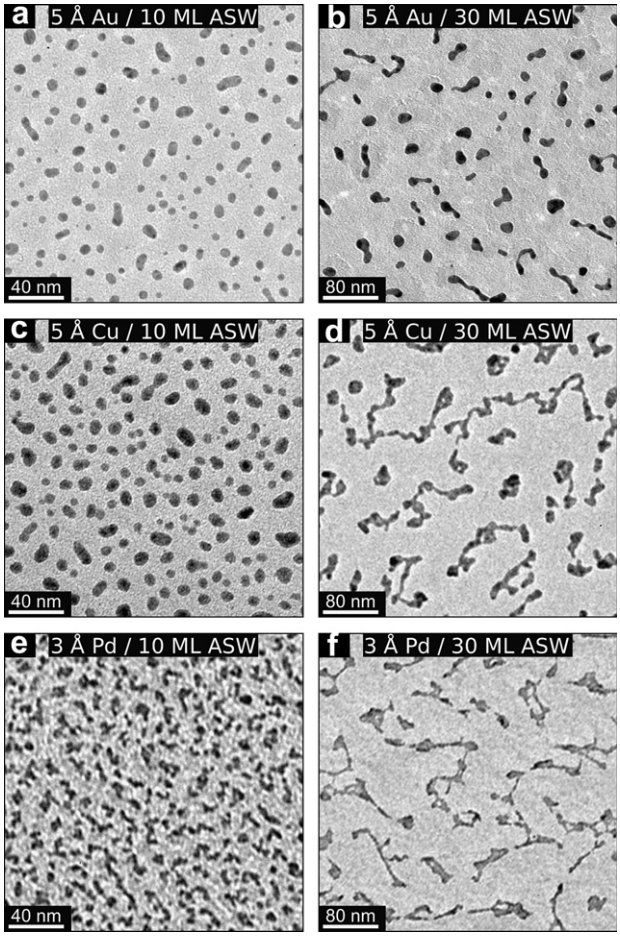

Fig. 1. Morphologies produced by the deposition of 5 Å of Au, 5 Å of Cu, and 3 Å of Pd on ASW buffers of 10 and 30 nm. Particle aggregation increases with buffer thickness, and the shapes of the particles are strongly dependent upon the coalescence properties of the metals.

completely coalesced. By comparison, the Pd particles in (e), where less material was deposited, are ramified. The Cu structures show an intermediate degree of coalescence.

Fig. 2 plots the densities of particles for deposition of 5 Å of Au on ASW films that ranged in thickness from 4 to 90 ML. The solid

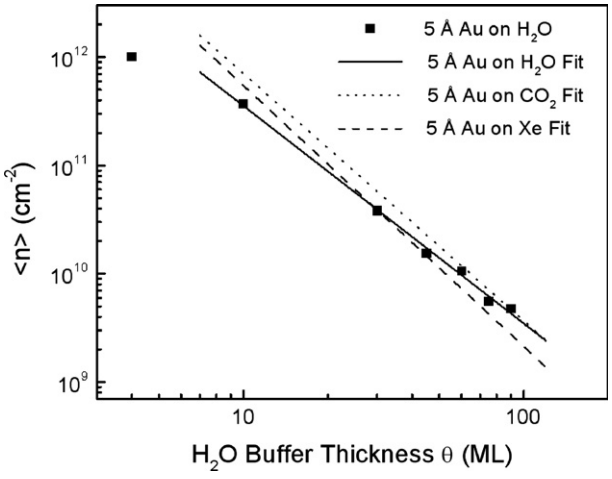

Fig. 2. Particle densities following 5 Å Au depositions onto ASW buffers of different thicknesses. The solid line shows a power law fit. The dashed and dotted lines are fits from Xe and CO_2 buffers from Refs. [16,17].

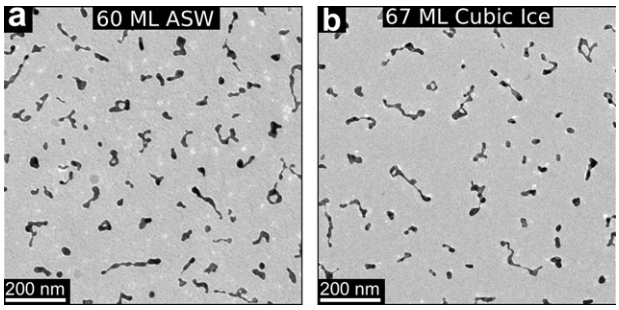

Fig. 3. TEM images for 5 Å of Au deposited on (a) 60 ML ASW and (b) 67 ML I_c. The resulting sizes and shapes are similar, and their particle number densities are consistent with the trend for ASW buffers shown in Fig. 2.

line fit shows a power law dependence on the buffer thickness with an exponent of 2.01 ± 0.06. Similar fits for 5 Å of Cu and 3 Å of Pd on ASW yield values of 2.17 ± 0.16 and 2.71 ± 0.20, respectively (not shown). As the densities drop with increasing buffer thickness, the sizes of the particles follow a power law increase in area and average radius (defined as average distance from the centroid to the perimeter), as reported for BLAG on Xe [9].

The densities of Au particles deposited on ASW follow the same trends as Au deposited onto Xe and CO_2 buffers. As shown by the dotted and dashed lines in Fig. 2 from Refs. [16,17], the differences are relatively small when considering the very large differences in desorption temperatures, and therefore the temperatures at which cluster aggregation occurs. The desorption temperatures, defined by the temperature at which the desorption rate is 1 ML/s, are 71, 86, and 165 K, for Xe, CO_2, and H_2O, respectively.

Fig. 3 shows particles formed on ASW and I_c buffers. Those in Fig. 3a were formed using a 60 ML buffer condensed at 20 K. Those in Fig. 3b were produced using a 67 ML buffer condensed at 135 K. Films condensed at 135 K are expected to be crystalline, while those produced at 20 K are very porous ASW [11]. The particle number density dropped from $1.1 \times 10^{10}/\text{cm}^2$ for ASW to $7.0 \times 10^9/\text{cm}^2$ for I_c, while the average area increased from 632 to 832 nm^2. These differences are consistent with expected changes for a slight increase in the buffer thickness, as shown in Fig. 2. While one might expect that the nucleation of particles on a porous ASW film would be significantly different than on a crystalline surface, any consequences of such nucleation are not evident in the final aggregated particles.

4. Solid water morphology changes during heating

The morphologies of water films grown from the vapor are highly dependent on the growth conditions. Because of kinetics, ASW films condensed at 20 K are rough on a short scale, but films grown at higher temperature will have much greater variation on a longer length scale. Condensation at 20 K results in a porous, yet uniformly thick film. Water molecules condensed on a-C at 135 K are mobile and multi-layer islands are formed. These islands grow together beyond a nominal condensation of ~30 ML.

ASW films will form I_c during warming, a process controlled by the structure of the film. The nucleation and crystallization rates will determine the structure of the film, and the rate of nucleation of I_c crystals depends on the deposition technique [18] and temperature [19]. Insight into these morphological changes is important to understand the interactions of particles with these films.

To investigate the mechanism behind particle aggregation on solid water, we began by studying the morphologies of the film during sublimation. Because the particle sizes and densities are sensitive to film thickness, we can use BLAG to probe changes that occur during heating. Fig. 4a is a TEM micrograph of particles formed by depositing 1 Å of Au on 30 ML of ASW. The sample in Fig. 4b was prepared the same way except that the Au was deposited during the warm-up process when the sample reached 153 K. In the latter case, the temperature of the substrate increased ~0.5 K during the 15 s deposition. At this stage, only ~3 ML would have sublimed, as determined by the area under the pressure vs. time curve. In Fig. 4, the local densities and size distributions are indicative of the film thickness when deposition occurred. Lower density regions manifest where the residual film was thickest. The oval region surrounded by the dotted line indicates a region where all of the Au had coalesced into a single particle. Just outside the oval is a region of small, high-density particles. These particles are consistent with Au deposited directly onto a-C when there was no buffer layer, i.e., regions where dewetting had occurred prior to Au deposition at ~153 K.

The reason for this particle distribution can be understood in terms of the crystallization process. An ice crystal nucleated inside the oval and grew by accumulation of H_2O from the surrounding area. This resulted in a depleted region around the crystal. The oval marks the footprint of the crystal at 153 K. The diffusion and crystallization of ASW results in roughening of the surface; such roughening is evident in Fig. 4b by the spatial variations in size and densities. It is consistent with previous observations that significant structural changes occur during crystallization that compromises the integrity of the film [20].

As the temperature increases during sublimation, further dewetting occurs and the film breaks up into islands. Fig. 4c shows the resulting morphology for a 30 ML ASW film that was heated to 160 K. As in Fig. 4b, Au was deposited during sublimation. While only ~5 ML of H_2O had sublimed at this point, there were significant changes to the film. The dashed lines indicate regions where islands formed. Au deposited onto them led to the formation of sin-

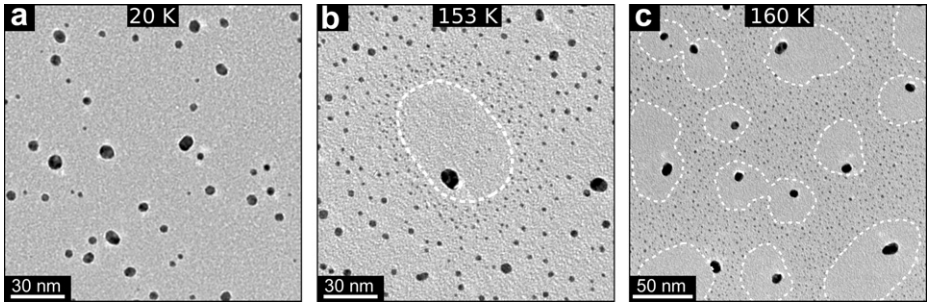

Fig. 4. Au particles formed by deposition of 1 Å of Au onto 30 ML ASW films. The Au was deposited at (a) 20 K or during H_2O restructuring and desorption at (b) 153 K or (c) 160 K. At 153 K, an ice crystal formed in the oval region identified in (b), depleting water from the surrounding area. Gold deposition onto a-C in the depleted region produced small high-density particles. Deposition at 160 K onto the islands marked by the dotted lines in (c) resulted in large particles while deposition onto the dewet areas resulted in small, high-density particles.

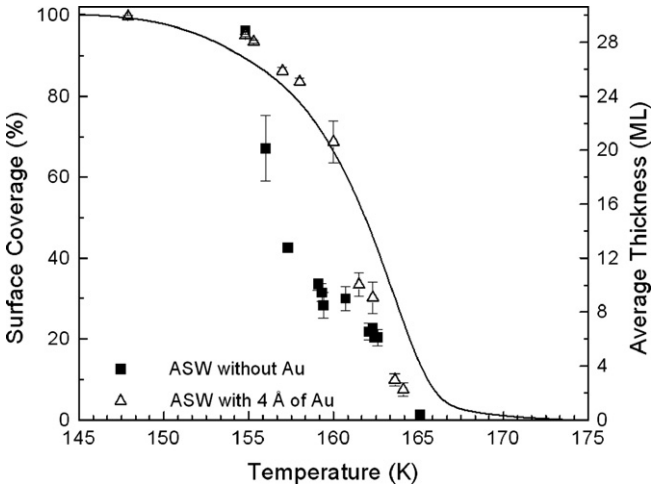

Fig. 5. Solid water coverage of the a-C surface at different temperatures (markers) and the average thickness during sublimation (line). Coverages were determined from images like those in Fig. 4 and the thickness was determined from integrating the time vs. pressure curve. Above 155 K, the film dewets to form islands, as shown by the steep drop in the surface coverage of the closed data points. After briefly leveling off, the coverage continues to drop as the islands decrease in size due to sublimation. The higher coverages exhibited by the open data points indicates that Au deposited on the film impedes dewetting.

gle particles. Outside the lines, Au atoms were directly deposited onto the a-C substrate exposed by islanding, and they grew into small, high-density particles.

Dewetting and sublimation occur simultaneously. Fig. 5 plots the H_2O surface coverage and its average thickness as a function of temperature. The coverages given by the squares were determined by analysis of images like those in Fig. 4. Those given by the triangles will be discussed later. The line shows the average thickness estimated from the area under the pressure vs. time curve. The formation of voids that spread and led to islanding accounts for the sudden drop in coverage at ~156 K. After the onset of dewetting, the coverage decreases more gradually at ~160 K, indicating that islanding is complete and further reduction can be attributed to sublimation. Once formed, the islands can break apart during sublimation, as seen by those that resulted in two particles in Fig. 4c. Note that the coverage drops to zero before all the water has desorbed; this is an artifact of our technique not having enough resolution to observe a few monolayers of H_2O.[2]

Although influenced by crystallization and the glass transition, dewetting is not dependent solely upon them. We have also observed thermally activated dewetting of thin crystalline ice films on a-C due to grooving at grain boundaries that leads to void formation. Fig. 6 shows the results of depositing 1 Å of Au at 157 K on a 57 ML ice film condensed at 140 K. After condensation, the film was cooled to 20 K and then warmed, as with the other samples. This growth sequence eliminated effects related to crystallization or the glass transition. The particle size distribution indicates that ice films dewet, with islanding in Fig. 6 at a stage between that in Fig. 4b and c.

The islanding of ASW films is not unexpected. Dewetting on a-C has previously been observed with TEM [13], and other studies show significant diffusion when ASW is heated above its glass transition [12]. Crystallization also causes structural changes in the film [20]. Moreover, solid state dewetting has been observed in thin metal [21] and ceramic films [22]. It occurs after a void that

[2] The resolution for determining the dewet/covered areas of the surface is limited by the spacing between particles deposited on the a-C, namely ~5 nm. The dewetting front continues to move as the Au is deposited. As I_c layers become thinner, it is difficult to distinguish particles deposited on a-C from those deposited onto H_2O. It is also not possible to determine how much water coats a particle.

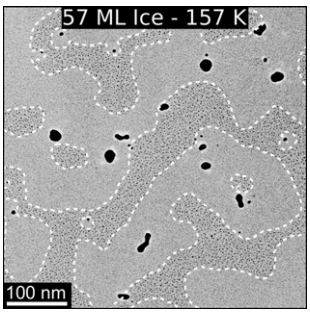

Fig. 6. Au particles formed by 1 Å of Au deposited on a 57 ML ice film condensed at 140 K. The Au was deposited at 157 K. The ice film had dewet, with islanding at a stage between those shown in Fig. 4b and c. The dotted lines indicate the boundaries between the exposed substrate and the ice islands, as in Fig. 4c.

extends to the substrate nucleates through thermal grooving at grain boundaries. Whether a void will grow and the film will dewet is determined by the interface and surface energies. Void growth ultimately results in film break up.

5. Particle aggregation on a dewetting film

Recent observations of Au particles on Xe indicate that capillary forces are responsible for aggregation during solid state dewetting and sublimation of the buffer [23]. The results of this study indicate a similar process for particle aggregation on H_2O. This is in contrast to earlier models for cluster aggregation during BLAG that assumed an ideal surface on which clusters could diffuse [16], with the grain structure and grooving introducing only slight perturbations [24]. These results are closer to the model proposed by Yan et al. [5] for Ag cluster formation on a ~3 ML ice layer that involved the formation of liquid droplets that swept along the Ag clusters and led to aggregation during desorption, but we have no indication of a liquid phase at 150 K.

To investigate the interaction of particles with dewetting ASW, we performed two-step evaporation sequences. First, we deposited 4 Å of Au on a 30 ML ASW film at 20 K and removed the sample from the cold head, as in our typical BLAG experiments. When the temperature reached 155 K, we deposited another 1 Å of Au and allowed the film to continue to sublime. Fig. 7a shows the result. The marked regions indicate that water had dewet so that the Au from the second evaporation formed small clusters on the exposed a-C substrate. Significantly, those particles formed during the initial 4 Å deposition retreated with the dewetting film. As for Au on Xe, it is reasonable to assume that the clusters sink partially into the solid water film to reduce surface energy. As the film dewets through molecular diffusion and H_2O overgrows the

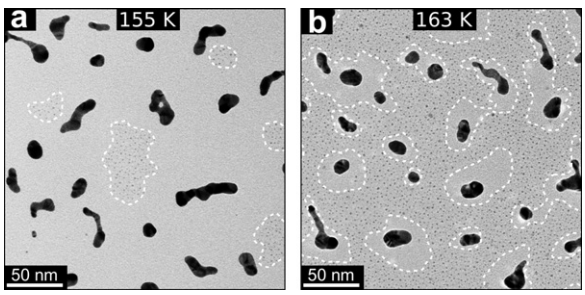

Fig. 7. Structures formed by deposition of 4 Å of Au onto 30 ML films of ASW at 20 K. In a second evaporation, 1 Å was added at (a) 155 K and (b) 163 K during desorption. The second evaporation produced small particles that delineate the boundaries of the still intact ice, as identified by the dotted lines. The observation of large Au particles entirely outside the dewet regions (none are bounded by small clusters) indicates that they were swept along with the dewetting film.

Table 1
Comparison of the aggregation/coalescence tendencies of Au, Cu, and Pd to the desorption properties of H_2O on those metals

Material	Power law exponent	% Surface coverage	Desorption peak shift (K)	
			(111)	(110)
5 Å Au	2.01	7.3	0 (Ref. [26])	5 (Ref. [27])
5 Å Cu	2.17	9.4	0 (Ref. [28])	10 (Ref. [29])
3 Å Pd	2.70	12.7	15 (Ref. [30])	50 (Ref. [31])

The desorption peak shift refers to the temperature of the final ML desorption peak with reference to the 150 K multilayer peak for single crystal surface. The surface coverage is averaged for particles produced on solid water films of 60 ML and greater.

particles, capillary forces move the particles with the dewetting front. Particles are initially concentrated along the front, but they aggregate as the solid water islands shrink due to sublimation. Accordingly, their sizes, shapes, and densities are related to the sizes, shapes, and densities of the islands.

In a second set of experiments, we prepared samples as for Fig. 7a except that the final 1 Å was deposited at 163 K, allowing the film to have exposed more of the a-C substrate. Fig. 7b shows that all of the initial 4 Å of Au has been concentrated into extended particles. This demonstrates the relationship between the island size and shape (dotted lines) and the final particle size and shape within the areas covered by solid water.

Comparison of Fig. 7b with Fig. 4c suggests that Au deposited on the ASW film affects dewetting, with the 4 Å of Au deposited at 20 K inhibiting dewetting. Dewetting is governed by the molecular diffusion of water. The triangles in Fig. 5 indicate coverages for samples prepared like those in Fig. 7, with the final 1 Å deposited at higher temperatures. The difference between the triangles and squares demonstrates that the particles slow down diffusion and dewetting. However, when sublimation is taken into account, inhibiting the diffusion leads to a thinner film, a decrease in the island size, and an increase in the island density.

Different nanoparticles will have different impacts on H_2O diffusion, reflecting their interactions with water. Table 1 lists the power law decay exponents for the densities and the percent surface coverage for Au, Cu, and Pd particles along with the interaction of water with their (111) and (110) surfaces. The table indicates the increase in the maximum desorption temperature for one monolayer compared to the multilayer desorption peak. Higher temperatures indicate a stronger interaction. The stronger interaction is manifest both in the variation in particle densities and particle surface coverages. A stronger interaction leads to a steeper power law decay because H_2O diffusion is inhibited, slowing void nucleation and growth. The coverage measures how much coalescence has occurred. Increased coalescence results in a lower surface coverage. Particles can become coated with a layer of H_2O, which will inhibit coalescence and result in more ramified structures. The impact of the water–metal interaction is evident in Fig. 1.

The interaction of the particles with the buffer varies significantly with the buffer material. The similarities among the densities of Au on Xe, CO_2, and H_2O shown in Fig. 2 suggest a scaling behavior between the particle–buffer interaction and the desorption temperature of the buffer. The scaling of the interaction energy with the cohesive energy of the buffer results in similar particle sizes and densities for a wide range of desorption temperatures and interaction energies.

6. Comparison of solid water to Xe

Comparison of the metal structures produced on H_2O films with those produced on Xe suggests that the particle aggregation processes are very similar. Both are driven by the dewetting of the film, but the particle interactions with the dewetting front show some key differences. Dewetting in Xe films leads to fingering [23] in a manner similar to the islanding of metal films [25]. These fingers eventually pinch off, and the process continues. A consequence is that particles are left behind the dewetting front. The equivalent is not observed on H_2O films, since no particles were left behind in the dewet regions in Fig. 6 and all the Au was concentrated onto the water islands.

Two features could contribute to the prevention of fingering of H_2O films. One, the stronger surface tension of water prevents fingering from occurring. This would keep Au particles moving with the front, allowing them to form larger structures than those observed on Xe. Second, the ASW films develop a much higher density of voids. The higher the void density, the shorter the distance the dewetting fronts must travel during islanding and the less chance there is for finger formation. Particle sizes from Xe and ASW films are similar, while the void density is significantly higher for ASW than Xe films ($\sim 6 \times 10^8$ for 5 Å of Au on a 20 ML Xe films and $\sim 4 \times 10^9$ for 4 Å Au on 30 ML ASW). This indicates that the void formation is more important than the change in surface tension. The ASW films break up into much smaller islands than the Xe films made up of large low energy grains. This structural difference inhibits fingering of ASW films. Even with this difference, the resulting structures produced on Xe and ASW films are very similar.

7. Conclusions

We have demonstrated that metals deposited on thin ASW films on a-C form particles that aggregate during dewetting and islanding. Dewetting is observed by depositing Au during heating. Deposition onto continuous films results in a homogeneous size distributions, while deposition onto dewet films results in an inhomogeneous size distribution. Dewetting occurs regardless of whether the film is amorphous or crystalline, although the mechanisms involved in void nucleation may change. Because aggregation occurs during dewetting near the sublimation temperature, deposition onto structurally different porous ASW and crystalline ice results in similar particles. The sizes of the dewetting islands affect the sizes and shapes of the resulting particles, and the metal interaction with the water affects the dewetting and the aggregation/coalescence of the structures. This dewetting-driven process is similar to that observed on Xe films, and we expect it to be a general process with small particles on thin volatile films since complete wetting of condensed gasses on surfaces is a rare occurrence [32]. In particular, recent observations indicate that ASW also dewets Pt(111) [33], Pd(111) [33], and Ru(0001) [34] during crystallization, leaving a monolayer, while Ni(111) provides a counter example where dewetting does not occur [35].

Acknowledgments

Early stages of this work were supported by the US Department of Energy, Division of Materials Sciences under Grant No. DEFG02-01ER45944. TEM imaging was carried out in the Center for Microanalysis of Materials, University of Illinois, which is partially supported by the US Department of Energy under Grant DEFG02-91-ER45439. We thank P. Swaminathan for stimulating discussions.

References

[1] P.G. Debenedetti, H.E. Stanley, Phys. Today 56 (6) (2003) 40.
[2] P.A. Thiel, T.E. Madey, Surf. Sci. Rep. 7 (1987) 211.
[3] M.A. Henderson, Surf. Sci. Rep. 46 (2002) 1.
[4] E. Gross, Y. Horowitz, M. Asscher, Langmuir 21 (2005) 8862.

[5] X.-M. Yan, J. Ni, M. Robbins, H.J. Park, W. Zhao, J.M. White, J. Nanoparticle Res. 4 (2002) 525.
[6] G. Liang, S.S. Perry, Surf. Sci. 594 (2005) 132.
[7] G.D. Waddill, I.M. Vitomirov, C.M. Aldao, J.H. Weaver, Phys. Rev. Lett. 62 (1989) 1568.
[8] L. Huang, S.J. Chey, J.H. Weaver, Phys. Rev. Lett. 80 (1998) 4095.
[9] C.L. Haley, J.H. Weaver, Surf. Sci. 518 (2002) 243.
[10] V.F. Petrenko, R.W. Whitworth, Physics of Ice, Oxford University Press, Oxford, England, 1999.
[11] K.P. Stevenson, G.A. Kimmel, Z. Dohnalek, R.S. Smith, B.D. Kay, Science 283 (1999) 1505.
[12] R.S. Smith, B.D. Kay, Nature 398 (1999) 788.
[13] P. Jenniskens, S.F. Banham, D.F. Blake, M.R.S. McCoustra, J. Chem. Phys. 107 (1997) 1232.
[14] D.E. Brown, S.M. George, C. Huang, E.K.L. Wong, K.B. Rider, R.S. Smith, B.D. Kay, J. Phys. Chem. 100 (1996) 4988.
[15] P. Jensen, Rev. Mod. Phys. 71 (1999) 1695.
[16] V.N. Antonov, J.S. Palmer, P.S. Waggoner, A.S. Bhatti, J.H. Weaver, Phys. Rev. B 70 (2004) 045406.
[17] P.S. Waggoner, J.S. Palmer, V.N. Antonov, J.H. Weaver, Surf. Sci. 596 (2005) 12.
[18] D.J. Safarik, C.B. Mullins, J. Chem. Phys. 121 (2004) 6003.
[19] J.M.K. Donev, Q. Yu, B.R. Long, R.K. Bollinger, S.C. Fain Jr., J. Chem. Phys. 123 (2005) 044706.
[20] R.S. Smith, C. Huang, E.K.L. Wong, B.D. Kay, Phys. Rev. Lett. 79 (1997) 909.
[21] C.M. Kennefick, R. Raj, Acta Metall. 37 (1989) 2947.
[22] D.C. Agrawal, R. Raj, Acta Metall. 37 (1989) 2035.
[23] J.S. Palmer, P. Swaminathan, S. Babar, J.H. Weaver, Phys. Rev. B. 77 (2008) 195422.
[24] J.S. Palmer, V.N. Antonov, A.S. Bhatti, P. Swaminathan, P.S. Waggoner, J.H. Weaver, Surf. Sci. 595 (2005) 64.
[25] E. Jiran, C.V. Thompson, Thin Solid Films 208 (1992) 23.
[26] B.D. Kay, K.R. Lykke, J.R. Creighton, S.J. Ward, J. Chem. Phys. 91 (1989) 5120.
[27] D.A. Outka, R.J. Madix, J. Am. Chem. Soc. 109 (1987) 1708.
[28] B.J. Hinch, L.H. Dubois, J. Chem. Phys. 96 (1992) 3262.
[29] K. Bange, D.E. Grider, T.E. Madey, J.K. Sass, Surf. Sci. 137 (1984) 38.
[30] M. Wolf, S. Nettesheim, J.M. White, E. Hasselbrink, G. Ertl, J. Chem. Phys. 94 (1991) 4609.
[31] J.W. He, P.R. Norton, Surf. Sci. 238 (1990) 95.
[32] J. Krim, J.G. Dash, J. Suzanne, Phys. Rev. Lett. 52 (1984) 640.
[33] G.A. Kimmel, N.G. Petrik, Z. Dohnalek, B.D. Kay, J. Chem. Phys. 126 (2007) 114702.
[34] S. Haq, A. Hodgson, J. Phys. Chem. C 111 (2007) 5946.
[35] M.E. Gallagher, S. Haq, A. Omer, A. Hodgson, Surf. Sci. 601 (2007) 268.